ACS APPLIED MATERIALS & INTERFACES

Research Article

www.acsami.org

Particle-Assisted Semidirect Breath Figure Method: A Facile Way to Endow the Honeycomb-Structured Petri Dish with Molecular Recognition Capability

Zhengkai Tu,[†] Haolin Tang,*[,†] and Xiantao Shen*[,‡]

[†]State Key Laboratory of Advanced Technology for Materials Synthesis and Progressing, Wuhan University of Technology, Wuhan 430070, China

[‡]G&T Septech, P.O. Box 33, N-1917 Ytre Enebakk, Oslo, Norway

Supporting Information

ABSTRACT: Recently, we have developed a semidirect breath figure (sDBF) method for direct fabrication of large-area and ordered honeycomb structures on commercial polystyrene (PS) Petri dishes without the use of an external polymer solution. In this work, we showed that both the pore size and the pore uniformity of the breath figure patterns were controllable by solvent amount. The cross-sectional image shows that only one layer of pores was formed on the BF figure patterns. By combing the sDBF method and Pickering emulsion and using the modular building blocks, we endowed the honeycomb-structured Petri dish with molecular recognition capability via the decoration of molecularly imprinted polymer (MIP) nanoparticles into the honeycomb pores. The radioligand binding experiments show that the MIP nanoparticles on the resultant honeycomb structures maintained high molecular binding selectivity. The reusability study indicates that MIP-BF patterns had excellent mechanical stability during the radioligand binding process. We believe that the modular approach demonstrated in this work will open up further opportunities for honeycomb structure-based chemical sensors for drug analysis, substrates for catalysts, and scaffold for cell growth.

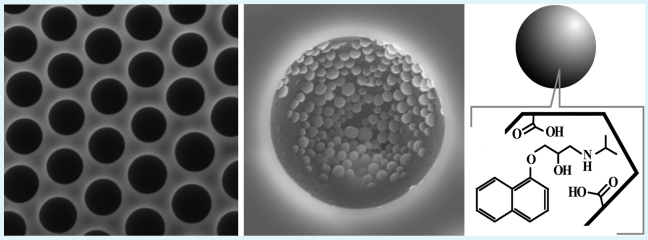

KEYWORDS: *semidirect breath figure, honeycomb structures, Petri dish, Pickering emulsion, molecular imprinting, molecular recognition*

1. INTRODUCTION

The Petri dish is a crucial piece of lab equipment in the microbiology lab, because the therapeutic protein, RNA, and genomic DNA samples are always produced by cell culture.[1] Recently, preparation of a Petri dish which provides a three-dimensional (3D) environment as the cells behave in vivo is a great challenge.[2] In the literature, the use of porous polymeric scaffolds to control the cell growth on surfaces has become an intensifying field in cell culture. For example, Recknor et al. studied the directional growth and differentiation of rat hippocampal progenitor cells on micropatterned polymer substrates. The 3D cell−cell environment could selectively control the neuronal differentiation and neurite alignment on topographically different regions of the same substrate.[3] Groves et al. reported the adhesion and growth of cells on solid membranes could be modulated by coating phospholipid. Culturing cells on these modified substrates indicated that fluid lipid bilayers generally blocked cell adhesion with a notable exception provided by membranes with phosphatidylserine.[4] Recently, Beattie et al. synthesized honeycomb-structured porous films using with customized amphiphilic block copolymers via the breath figures (BF) method. The obtained films were noncytotoxic and hence suitable as porous substrates for tissue engineering.[5] Using the BF method, polystyrene-*b*-polybutadiene-*b*-polystyrene[6] and multifunctional amphiphilic biodegradable copolymers[7] have also been used as polymer to construct ordered honeycomb scaffolds for cells.

The BF method has attracted increasing attentions for fabrication of culturing scaffolds because of its advantages (e.g., facile operation, low cost, solid mechanism of film formation, and large-area pattern).[8,9] The term of the traditional breath figure refers to the arrangement of condensed water droplets on a polymer solution on silicon wafers, quartz, mica, metals, indium tin oxide, TEM grids, plastics, and water.[10,11] During the fabrication of the BF arrays, the casting conditions (e.g., polymer nature, polymer concentration, solvent, casting volume, relative humidity, and temperature) could be used to control the ordered holes within a size range of 300 nm to 20 μm.[12,13] To avoid using an external polymer solution, Farbod et al. recently reported an improved direct breath figure (DBF) method to pattern breath figures on poly(methyl 2-methyl-propenoate) (PMMA) substrates.[14] The figure was indeed part of the substrate, which increased the stability of the film. However, the BF patterns obtained via DBF were not ordered.

Received: May 9, 2014
Accepted: June 18, 2014
Published: June 18, 2014

Most recently, we developed a semidirect breath figure (sDBF) method to directly prepare large-area and ordered honeycomb structures on polymer substrates by combination of the normal breath figure (NBF) method and the DBF method.[15] During the synthesis, pure solvent (chloroform) was directly cast on a polystyrene (PS) Petri dish. Compared to the NBF method, there were two main benefits to the sDBF method: (i) the synthesized honeycomb structure was indeed part of the substrate, which provides the BF patterns with enough mechanical strength; (ii) large-area and ordered honeycomb structure could be patterned on the substrates because the polymer solution is free in the present method.[16]

To gain new insights in cell information, analysis of a target molecule from the culture system has become more and more important. For example, bacteria communicate with one another using chemical signal molecules. Monitoring the target molecules is critical for understand how chemical information is integrated, processed, and transduced to control gene expression.[17] Recently, selective extraction of a target compound from a complex culture system is playing an increasingly important role in molecular microbiology, toxicological testing, diagnostic biomarker discovery, and drug discovery and development.[18] Therefore, fabrication of a Petri dish with high molecular recognition capability is another great challenge in cell culture.[19]

Recently, Lu et al. reported the synthesis honeycomb-structured substrates with molecular recognition capability.[20] Using poly(styrene-*stat*-acrylonitrile-*stat*-vinyl-2,4-diamino-1,3,5-triazine) as functional polymers and poly(styrene-*stat*-acrylonitriles) as matrix polymers, they prepared a type of molecularly imprinted polymer (MIP) membranes via a water-assisted method. The experimental results showed that the MIP membranes effectively recognized the template molecule. In molecular imprinting, MIPs are always synthesized by the copolymerization of the functional monomers and cross-linkers in the presence of template molecules.[21,22] Because of the higher surface area of the MIP particles compared to bulk MIPs,[23,24] MIP particles possess more accessible molecular binding sites and have been used as modular particles to generate functional composite materials.[25,26] In this work, we will decorate the MIP nanoparticles in the pores of the honeycomb-structured Petri dish during the sDBF process, which leads the Petri dish to highly specific molecular recognition capability. The decoration of the MIP nanoparticles was conducted by self-assembly of polymer and MIP nanoparticles mixture at the oil−water droplet interface. This polymer and MIP nanoparticles blend-assisted fabrication is a procedure combining the so-called "Pickering emulsion"[27,28] and BF processes. The complete evaporation of the solvent and water confines the MIP nanoparticles assembly into the walls of the honeycomb arrays.

The present method for the synthesis of a honeycomb-structured Petri dish decorated with MIP nanoparticles displays two interesting aspects. First, we have previously proved that the cell attachment on pores of the honeycomb-patterned Petri dishes was enhanced because of the hydrophobic interaction.[15] Second, the MIP nanoparticles decorated in the Petri dish could selectively recognize the target compounds, and thus the Petri dish could be used as highly efficient adsorbents. As far as we are aware this is probably the first report of the pattern of MIP honeycomb structures in a Petri dish and could offer new insights in surface engineering with a high potential for application in commercial technologies. The details of the investigation are presented below.

2. EXPERIMENTAL SECTION

2.1. Materials. Methacrylic acid (MAA, 98.5%) was purchased from ACROS (Geel, Belgium). Azobis(isobutyronitrile) (AIBN, 98%) was purchased from Merck (Darmstadt, Germany). Trimethylolpropane trimethacrylate (TRIM, technical grade) and atenolol (98%) were purchased from Sigma-Aldrich (Gillingham, U.K.). *N*-Isopropylacrylamide (NIPA) and *N*,*N*′-methylene-bisacrylamide (MBAAm) were purchased from Monomer-Polymer Laboratories (Windham, U.S.A.). Fluorescein isothiocyanate (FITC, ≥90%), acrylamide and (*R*,*S*)-propranolol hydrochloride (99%) were supplied by Fluka (Dorset, U.K.). [^{3}H]-(*S*)-Propranolol (specific activity 555 GBq mmol^{-1}, 66.7 μM in ethanol solution) was purchased from NEN Life Science Products, Inc. (Boston, MA). The scintillation liquid Ecoscint A was obtained from National Diagnostics (Atlanta, GA). Nunclon cell Petri dishes (polystyrene, Mw ∼220 000, 3.5 cm in diameter) were purchased from Sigma-Aldrich. AIBN was recrystallized from methanol before use. Other solvents were of analytical reagent grade and were used without further purification.

2.2. Preparation of Hydrophobic MIP-Core and Hydrophilic MIP-CS Nanoparticles. MIP nanoparticles were synthesized following a similar procedure described by Hajizadeh et al.[29] Briefly, 137 mg of (*R*,*S*)-propranolol, 113 mg of MAA, 648 mg of TRIM, and 28 mg of AIBN were dissolved in 40 mL of acetonitrile in a borosilicate glass tube. To remove the oxygen, the solution was purged with nitrogen for 5 min. The glass reactor was introduced into a hybridization oven (60 °C), and the tube was rotated at a speed of 20 rpm. The polymerization was conducted at 60 °C for 24 h. After reaction, the polymeric nanoparticles were collected by centrifugation. To remove the template, the polymeric nanoparticles were washed with methanol containing 10% acetic acid. The concentration of the remaining propranolol in the washing solvent was measured with a UV absorption spectrophotometry. When no template could be measured from the washing solvent, the polymeric nanoparticles were washed with water and methanol and dried in a vacuum chamber at room temperature. In this way, the propranolol-imprinted core nanoparticles (MIP-core nanoparticles) were synthesized. As a control, non-imprinted polymer nanoparticles (NIP-core nanoparticles) were also prepared using the same condition except that no template was added during the synthesis.

To coat a hydrophilic shell on the MIP-core (or NIP-core) nanoparticles, 40 mL of acetonitrile, 188 μL of allylamine, 566 mg of NIPA, 77.2 mg of MBAAm, 24 mg of AIBN, and 1000 mg of the polymeric particles were added into a borosilicate glass tube and sonicated for 3 min. After a standing at room temperature under a gentle flow of N_2 for 5 min, the mixture was kept at 60 °C under a gentle rotation of 20 rpm for 48 h. After polymerization, the polymeric nanoparticles with hydrophilic shell were separated by centrifugation. The MIP core-and-shell (MIP-CS) or NIP core-and-shell (NIP-CS) nanoparticles were washed with methanol and acetone and dried in a vacuum chamber at room temperature.

2.3. Preparation of Honeycomb Structures. The experimental setup for the fabrication of honeycomb structures on the PS Petri dishes has been described in our previous study.[15] Briefly, 1 mL of chloroform was cast into a PS Petri dish (3.5 cm in diameter). Immediately, the Petri dish was placed in a stream of water-saturated air (which was flowed through a two-stage water pass).[30] The relative humidity of the air flow was controlled at 75%. After solidification of 30 min, the Petri dish was dried at room temperature for 8 h.

2.4. Decoration of MIP Nanoparticles on Honeycomb Structures. To immobilize MIP nanoparticles on the honeycomb structures, 2 mg of MIP nanoparticles was added into 100 μL of acetonitrile. After a 5 min sonication, 1 mL of chloroform was added to this suspension. The mixture was thus used as "solvent" to form MIP honeycomb structures. Other steps were same to the preparation of normal honeycomb structures by the sDBF method in section 2.3.

When MIP-CS nanoparticles were used as modular nanoparticles to decorate the BF patterns, a cross-linking step was also conducted after drying of the Petri dish. Typically, 2 mL of water (pH 2) containing 0.5% glutaraldehyde was added into the Petri dish. The Petri dish was sealed and placed at 37 °C for 12 h. In this way, the MIP-CS nanoparticle was cross-linked covalently to one another, which will avoid losing of the MIP-CS nanoparticles from the Petri dish. To remove the remaining glutaraldehyde and block the free aldehyde groups, the Petri dish was washed with water, carbonate buffer (containing 4 g L^{-1} sodium borohydride), and water, respectively. The obtained honeycomb structures on the Petri dish decorated with MIP-CS nanoparticles was named MIP-BF patterns. As a reference, the honeycomb-structured Petri dish was also decorated with NIP-CS nanoparticles, which was named NIP-BF patterns.

2.5. Characterization. The surface morphology of the honeycomb structures and nanoparticles was observed by scanning electron microscope (SEM) on a Thermal field emission SEM LEO 1560 instrument (Zeiss, Oberkochen, Germany).

The surface groups of the MIP nanoparticles were investigated by Fourier transform infrared (FTIR) analysis using a PerkinElmer FTIR instrument (PerkinElmer Instruments). All spectra were recorded in the 4000−375 cm^{-1} region with a resolution of 4 cm^{-1} using 16 scans at room temperature.

The size of the MIP nanoparticles was determined using dynamic light scattering measurement (DLS) at 25 °C on a Zetasizer Nano ZS instrument equipped with a software package DTS ver. 4.10 (Malvern Instruments Ltd., Worcestershire, U.K.). Prior to particle size measurement, an aqueous solution containing 20 μg mL^{-1} MIP-CS nanoparticles was prepared.

2.6. Radioligand Binding Analysis. The MIP honeycomb structures containing MIP-CS nanoparticles (MIP-BF patterns) were cut into small pieces (~0.5 cm^2). All pieces and [^{3}H]-(*S*)-propranolol (246 fmol) were mixed in 2 mL of acetonitrile/citrate buffer (25 mM, pH 6.0) (50:50). For displacement experiments, an excess amount of competitor (atenolol or propranolol) was also added. The mixture was placed at room temperature for 12 h. After removal of the polymer substrates, 500 μL of the solution was mixed with 10 mL of scintillation liquid (Ecoscint A) and measured with a Tri-Carb 2800TR liquid scintillation analyzer (PerkinElmer). The amount of [^{3}H]-(*S*)-propranolol bound was obtained by subtracting the amount of free radioligand from the total radioligand added.[31,32]

3. RESULTS AND DISCUSSION

3.1. Synthesis of MIP-Core and MIP-CS Nanoparticles. In this study, two types of MIP nanoparticles were selected as modular nanoparticles for the decoration of the honeycomb-structured Petri dish: the hydrophobic MIP-core nanoparticles and the hydrophilic MIP core−shell (MIP-CS) nanoparticles. During the synthesis of MIP-core nanoparticles, the cross-linkers were 61% of the total monomers. This high ratio of cross-linkers was helpful for the formation of rigid and specific cavities. However, when we introduced a hydrophilic NIPA−allylamine−MBAAm shell on the MIP-core nanoparticles, the cross-linkers were only 6% of the total monomers. We have previously proved that the grafting of a copolymer layer onto MIP-core nanoparticles with low cross-linking did not affect the particle size and the MIP-core binding capability.[33]

During the coating of the hydrophilic shell, amine groups were introduced through copolymerization of NIPA, allylamine, and MBAAm monomers. In order to confirm the presence of the hydrophilic amino shell, the surface groups of the MIP-core and MIP-CS nanoparticles were studied by FTIR analysis (Figure 1). Compared to MIP-core nanoparticles, the MIP-CS nanoparticles coated with a NIPA−allylamine−MBAAm copolymer layer displayed obvious changes: (i) the N−H stretching band and bending vibration of allylamine primary amines were clearly shown at 3300 and 1595 cm^{-1}, respectively;[34,35] (ii) the peaks at 3085 and 2932 cm^{-1}, which are associated with the C−H stretching vibration, were disappeared; (iii) a new amide I band (C═O stretching) was emerged at 1638 cm^{-1}; this is due to the introduction of poly(NIPA) or poly(MBAAm) structure on the surface of the MIP-CS nanoparticles.[36] These FTIR results confirmed that the NIPA−allylamine−MBAAm copolymer had been successfully grafted onto the MIP-CS nanoparticles.

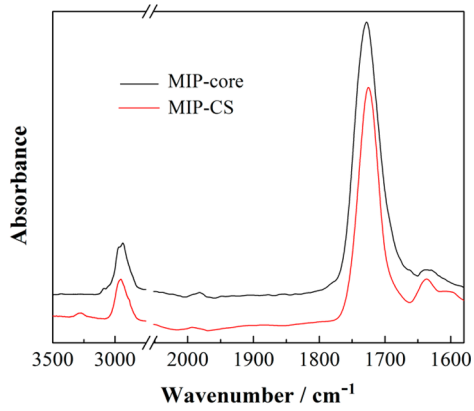

Figure 1. FTIR analysis of MIP-core nanoparticles and MIP-CS nanoparticles.

Previous work has demonstrated that the MIP-core nanoparticles synthesized with high percentage of TRIM were hydrophobic, while the MIP-CS nanoparticles containing a NIPA−allylamine−MBAAm shell were hydrophilic.[28] To confirm the surface nature, both the MIP-core and MIP-CS nanoparticles (25 mg) were dispersed in a mixture of water (0.8 mL) and toluene (0.8 mL). Figure 2 shows that poly(MAA-*co*-TRIM)-based MIP-core nanoparticles dispersed well in the toluene, while the MIP-CS nanoparticles dispersed well in the water phase because of their hydrophilic shell. This further indicates that the MIP-core particles had been converted into the core−shell structured nanoparticles.

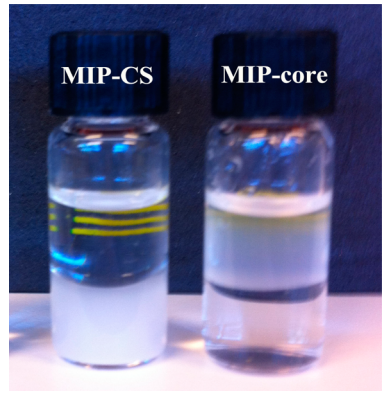

Figure 2. MIP-CS and MIP-core nanoparticles dispersed in a mixture of water and toluene. The MIP-CS nanoparticles partitioned into the water phase, while the MIP-core nanoparticles partitioned into the toluene phase.

The SEM image of the MIP-CS nanoparticles is shown in Figure 3a. It is seen that the diameter of the dry MIP-CS nanoparticles was 440 ± 109 nm. To further confirm the coating of hydrophilic layer on MIP-core nanoparticles, the particle size of the MIP-CS nanoparticles in aqueous solution was also determined by DLS. It is seen in Figure 3b that the

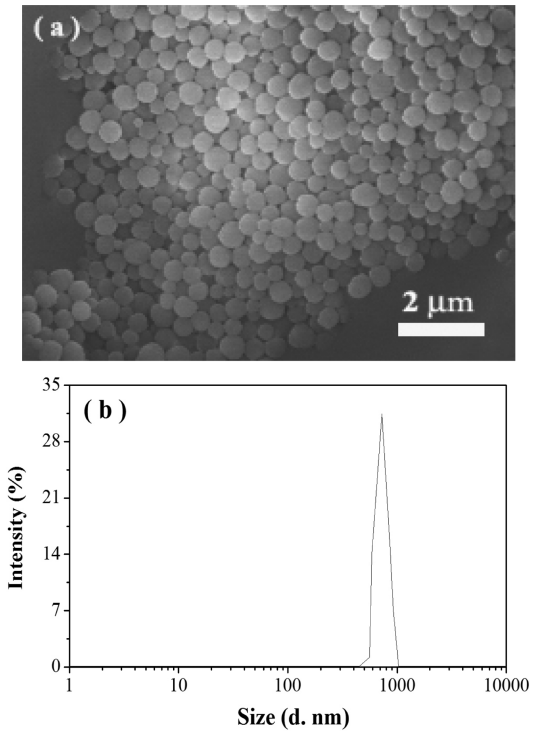

Figure 3. (a) SEM image of the dry MIP-CS nanoparticles. (b) Size distribution profile obtained by DLS for MIP-CS nanoparticle in an aqueous solution.

MIP-CS nanoparticles in aqueous solution had a hydrodynamic diameter of 723 nm. Obviously, because of the swelling of the hydrophilic shell and the introduction of the amine groups in water, the MIP-CS nanoparticles in aqueous solution displayed significantly larger size than the dry MIP-CS nanoparticles. These SEM and DLS analysis further confirmed the existence of a hydrophilic shell layer on MIP-CS nanoparticles.

3.2. Control Pore Size of the BF Patterns by Change of Solvent Amount. In an NBF method, the effect of the solution viscosity on the breath figure formation has been studied by Sharma et al.[37] It is generally accepted that a low viscosity resulted in disordered pattern arrays because of the coalescence of the water droplets. However, in a solution with high viscosity, the water droplets are difficult to diffuse across the interface, leading to fewer and bigger pores on the substrate. During the generation of breath figure using sDBF method, chloroform was used instead of a polymeric solution in an NBF method, and the amount of solvent would affect the evaporation time as well as the viscosity of the solution. Using a relative humidity (RH) value of 75%, the effect of solvent amount on breath figure formation was studied in this work. It is seen in Figure 4, parts c and d, that when a large amount of solvent was used in our method, the surface of the solution was pure solvent with low viscosity; the coalescence of the water droplets resulted in a disordered pattern arrays. On the other hand, larger amount of solvent needed longer time to evaporate; the number-averaged diameter of the pores (D_n) of the pores was thus larger. When a small amount of solvent was used, the viscosity of the solution increased very fast, which resulted the water droplets in difficult diffusion across the surface. Therefore, only a few irregular pores were presented on the breath figure pattern in Figure 4a. Whatever, we have shown here that both the pore size and the pore uniformity of the breath figure patterns are controllable by solvent amount. Using 1 mL of chloroform, an ordered porous array (D_n = 7.9 ± 0.02 μm) was successfully patterned on the Petri dishes.

To claim morphology controllability, the cross-sectional SEM images of patterned polymer substrate were always shown in the NBF method.[38] In an NBF process using PS in chloroform solution, coalescence between water droplets was seriously blocked when the condensed water droplets on the solution surface sink down, because the water droplets were stabilized by the polymer solution with high viscosity. After complete drying of the solvent, multilayered pores were usually formed in the upper part of patterns, whereas a solid bulk polymer was generated below the lowest layer of pores.[39] In this work, the cross section of breath figure patterns prepared by the sDBF method was also observed using optical microscopy. It is seen in Supporting Information Figure S1 that only one layer of pores was formed on the BF figure patterns prepared by the sDBF method. This can be explained as follows: In the sDBF process, pure chloroform was used instead of the polymer solution. When condensed water droplets (formed on the surface of chloroform) sink down, coalescence of these droplets was found because the viscosity of the pure chloroform was not strong enough to stabilize them. However, the PS concentration near the surface of the solid substrate increased very fast; thus, the concentrated polymer solution prevented the condensed water droplets from coalescence. After complete drying of chloroform, only one layer of pores (with larger pore size) can be formed at the surface of the BF patterns.

3.3. Preparation of MIP-BF Patterns. Honeycomb-structured substrates with uniform pores could be used as functional materials such as sensors.[40] Therefore, it is needed to endow the honeycomb-structured substrates with molecular recognition capability. Recently, MIPs have been reported to possess specific recognition ability toward preselected target molecules, which have been used in various fields. Thus, the combination of molecular imprinting and breath figure method

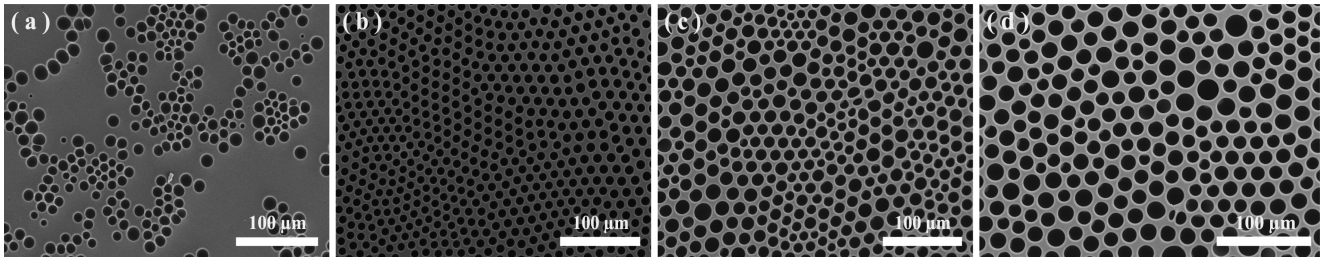

Figure 4. SEM images of BF patterns prepared under an RH value of 75% using different volumes of chloroform: (a) 0.5, (b) 1.0, (c) 1.5, and (d) 2.0 mL. Panel b reprinted from ref 15. Copyright 2014 American Chemical Society.

is a promising way to obtain honeycomb-structured substrates with molecular recognition capability. In breath figure method, solid particles would also assemble at the interface of water/solution under the action of Pickering emulsions effect.[41] Here, we endowed the honeycomb structures with molecular recognition capability by decoration of MIP nanoparticles. In the literature, physical and chemical properties of the nanoparticles have been reported to influence the honeycomb structures in an NBF process.[42] Among of the properties, the wettability of the nanoparticles is the most important factor to be considered in Pickering emulsions. In order to investigate the effect of the wettability of the MIP nanoparticles on the sDBF patterning procedure, both hydrophilic and hydrophobic MIP particles were used to prepare the MIP-BF patterns. The SEM image in Figure 5a and the close-up in Figure 5b reveal

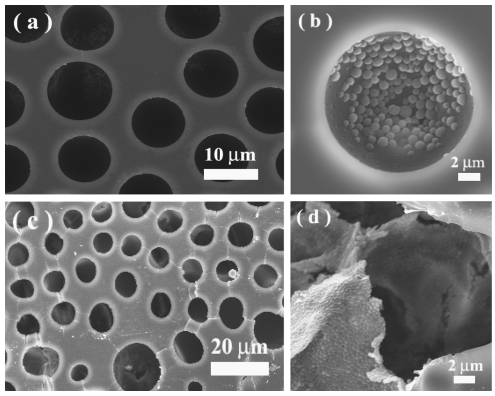

Figure 5. Honeycomb structures decorated with hydrophilic MIP-CS nanoparticles (a and b) and hydrophobic MIP-core nanoparticles (c and d).

that hydrophilic MIP-CS nanoparticles basically located on the pore walls. It is evident that, during the early stage of BF process, the hydrophilic property of the MIP-CS nanoparticles promotes them to distribute mainly in the water phase. While in the case of the hydrophobic nanoparticles (Figure 5c), the MIP-core nanoparticles display completely different assembling morphology. The close-up of the SEM image in Figure 5d shows that the MIP-core nanoparticles were assembled into the interior walls of the pores, because the hydrophobic nanoparticles distributed mainly in the oil phase. All these results agreed with the experimental study by Sun et al.[43] On the other hand, the size of the pore openings in Figure 5a (approximately 10 μm) is larger than that in Figure 4b, because the present of MIP-CS nanoparticles and acetonitrile in the emulsion decreased the interfacial tension between polymer solution and water droplets.[44]

The material surface designing strategy is very important for application of the patterns. To gain more information about the material surface designing strategy, fluorescence microscopy analysis and wetting properties of the patterns were studied. Supporting Information Figure S2 is the fluorescence microscopy of the BF patterns without nanoparticles and the MIP-BF patterns after a treatment of FITC. It is seen that the MIP-BF patterns displays generally higher fluorescence intensity that the BF patterns without nanoparticles; this is because of the presence of amino groups on the MIP nanoparticles of the MIP-BF patterns. Supporting Information Figure S3 shows the wetting properties of the different substrates. It is seen that the pure Petri dish had a water contact angle of 39°. After the patterns of the honeycomb structures, the rough surface results the BF patterns in an increasing of the water contact angle to 92°. When the MIP nanoparticles were introduced into the MIP-BF patterns, the water contact angle value of the substrate decreased to 33°. This change is due to the fact that (i) the pore size of the MIP-BF patterns was larger than that of the BF patterns without nanoparticles; (ii) the introduction of the hydrophilic MIP nanoparticles increased the hydrophilicity of the BF patterns. This hydrophilicity leads to the facile application of the MIP-BF patterns in the buffer system.

3.4. Molecular Recognition on MIP-BF Patterns. The MIP-BF patterns were evaluated for their specific binding by using tritium-labeled propranolol as a probe. As a control, the NIP-BF patterns (breath figure patterns prepared using NIP-CS nanoparticles) were used to investigate the nonspecific adsorption. It is known that molecular imprinting is mimicking an artificial tiny lock for a target molecule that serves as miniature key. During the recognition, the specificity of the MIPs was conferred by hydrogen bonding and shape selectivity. To avoid the surface hydrophilic/hydrophobic interaction (nonspecific binding), the binding experiment is conducted in a rigorous condition [citrate buffer (25 mM, pH 6.0)/acetonitrile]. Figure 6 shows the uptake of [^{3}H]-(*S*)-

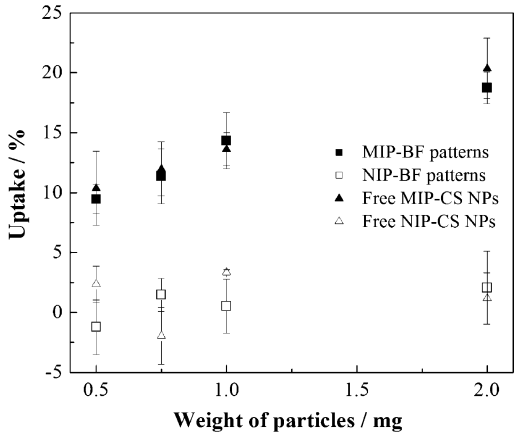

Figure 6. Uptake of propranolol (246 pM) by the MIP-BF patterns, NIP-BF patterns, free MIP-CS nanoparticles, and free NIP-CS nanoparticles (with 0.5, 0.75, 1.0, and 2.0 mg of nanoparticles) in 2 mL of citrate buffer (25 mM, pH 6.0)/acetonitrile (1:1, v/v).

propranolol by the MIP-BF patterns and the NIP-BF patterns through radioligand binding analysis. As shown in Figure 6, the radioligand uptake by the MIP-BF patterns was in general higher than the NIP-BF patterns, suggesting that the selectivity of the MIP-BF patterns is not attributed to the specific surface area and/or surface hydrophilic/hydrophobic interactions from the substrates. When the amount of the MIP-CS nanoparticles in the honeycomb structures was increased, the radioligand uptake by the MIP-BF patterns was also enhanced. However, the nonspecific binding, as reflected from the NIP-BF patterns, remained very low. In addition, the binding profile of the free MIP-CS nanoparticles was very similar to that of the MIP-BF patterns, suggesting the decoration of MIP-CS nanoparticles onto the Petri dishes did not decrease their specific binding capacity and this specific binding is directly originated from the MIP nanoparticles. Therefore, the MIP-BF patterns indeed displayed obvious specific binding for the template.

The molecular selectivity of the MIP-BF patterns was also confirmed by investigating their competitive radioligand binding. As shown in Figure 7, the addition of the competitors

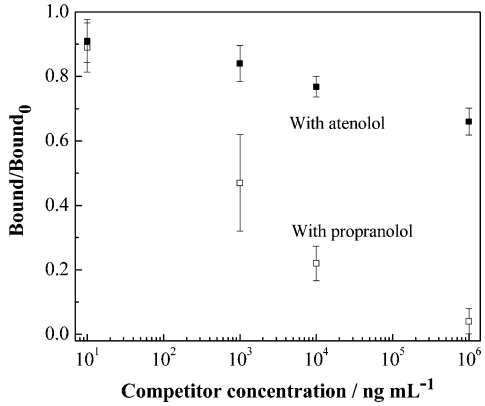

Figure 7. Competitive radioligand binding analysis of the MIP-BF patterns (decorating with 2 mg of MIP-CS nanoparticles) in 2 mL of citrate buffer (25 mM, pH 6.0)/acetonitrile (1:1, v/v). Here, Bound$_0$ and Bound are the amounts of [^{3}H]-(*S*)-propranolol bound by the nanoparticles in the absence and presence of the competing compounds, respectively.

both decreased the uptake of the MIP-CS nanoparticles on the MIP-BF patterns. However, the potency of atenolol (a structural analogue of propranolol) to displace the radioligand from the MIP honeycomb structures was significantly lower than the potency of (*S*)-propranolol. These experimental results further confirmed that the highly specific binding sites in the MIP-BF patterns remain easily accessible.

In the previous works, molecularly imprinted membranes were usually synthesized from the functional monomers.[45,46] Compared to these works, the present work reports a completely new way to synthesize molecularly imprinted membranes by using modular MIP nanoparticles as building blocks. The most important advantage of the present method is that the molecular recognition sites were always generated under the optimal imprinting condition.[33]

3.5. Reusability of MIP-BF Patterns. During the synthesis of MIP-BF patterns, the amino groups of the MIP-CS nanoparticles were cross-linked using glutaraldehyde to avoid the loss of the MIP-CS nanoparticles during the application. To exhibit the stability of the MIP-CS nanoparticles in the BF patterns, the reusability of the MIP-BF patterns (decorating with 2 mg of MIP-CS nanoparticles) was evaluated by analyzing their capability to bind the radioligand after several cycles of regeneration (Figure 8). In the first cycle, the radioligand binding experiment was conducted for 12 h. Then the MIP-BF patterns were simply recovered with a tweezer. The MIP-BF patterns were washed with methanol containing 10% acetic acid for three times to remove the radioligand, and then with methanol for three times to remove the acetic acid, respectively. After drying of the MIP-BF patterns, the radioligand binding experiment was continued again for 12 h as a second cycle. This process was repeated for five cycles. Compared to the fresh MIP-BF pattern, the regenerated MIP-BF patterns could be used at least for five times without decreasing the adsorption capacity. This indicates that the MIP-BF patterns have excellent mechanical stability during the radioligand binding process.

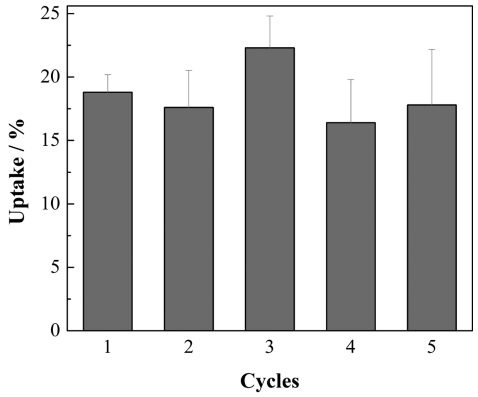

Figure 8. Reusability of MIP-BF patterns in successive batches of radioligand binding.

4. CONCLUSION

In this work, we showed that both the pore size and the pore uniformity of the breath figure patterns were controllable by solvent amount during the sDBF process. By combing the sDBF method and Pickering emulsion, we endowed the honeycomb-structured Petri dish with molecular recognition capability via the decoration of MIP nanoparticles into the honeycomb pores. The radioligand binding experiments show that the MIP nanoparticles on the resultant honeycomb structures maintained high molecular binding selectivity. The reusability study indicates that MIP-BF patterns had excellent mechanical stability during the radioligand binding process. This kind of the MIP honeycomb structures could be used as highly efficient adsorbents or catalysts for practical applications. We believe that the modular approach demonstrated in this work can be extended to conjugate honeycomb structures with other functional nanoparticle building blocks (e.g., quantum dots, catalysts, and cells) or reporter molecules. In our previous work, we have proved that the cell attachment on pores of the honeycomb-patterned Petri dishes was enhanced because of the hydrophobic interaction.[15] Therefore, the new materials presented here will open up further opportunities for honeycomb structure-based chemical sensors for drug analysis, substrates for catalysts, and scaffolds for cell growth.

■ ASSOCIATED CONTENT

Ⓢ Supporting Information

Supporting information including cross-sectional image of the BF patterns, fluorescence microscopy of the BF patterns, and the wetting properties of the BF patterns. This material is available free of charge via the Internet at http://pubs.acs.org.

■ AUTHOR INFORMATION

Corresponding Authors

*E-mail: thln@whut.edu.cn.
*E-mail: xtshenlab@gmail.com.

Notes

The authors declare no competing financial interest.

■ ACKNOWLEDGMENTS

This work is financially supported by the National Nature Science Foundation of China (51272200), Program for New Century Excellent Talents in University (NCET-12-0911), and the Fundamental Research Funds for the Central Universities (WUT: 2013-IV-037, 2013-II-011). Tripta Kamra in the

Division of Synchrotron Radiation Research, Lund University, Sweden is warmly acknowledged for the SEM measurement.

REFERENCES

(1) Zhang, S. Beyond the Petri Dish. *Nat. Biotechnol.* **2004**, *22*, 151−152.

(2) Pampaloni, F.; Reynaud, E. G.; Stelzer, E. H. K. The Third Dimension Bridges the Gap between Cell Culture and Live Tissue. *Nat. Rev. Mol. Cell Biol.* **2007**, *8*, 839−845.

(3) Recknor, J. B.; Sakaguchi, D. S.; Mallapragada, S. K. Directed Growth and Selective Differentiation of Neural Progenitor Cells on Micropatterned Polymer Substrates. *Biomaterials* **2006**, *27*, 4098−4108.

(4) Groves, J. T.; Mahal, L. K.; Bertozzi, C. R. Control of Cell Adhesion and Growth with Micropatterned Supported Lipid Membranes. *Langmuir* **2001**, *17*, 5129−5133.

(5) Beattie, D.; Wong, K. H.; Williams, C.; Poole-Warren, L. A.; Davis, T. P.; Barner-Kowollik, C.; Stenzel, M. H. Honeycomb-Structured Porous Films from Polypyrrole-Containing Block Copolymers Prepared via RAFT Polymerization as a Scaffold for Cell Growth. *Biomacromolecules* **2006**, *7*, 1072−1082.

(6) Zhao, W.; Lang, M.; Li, Y.; Li, L.; Shi, J. Robust and Hydrophilic Polymeric Films with Honeycomb Pattern and Their Cell Scaffold Applications. *J. Mater. Chem.* **2009**, *19*, 2789−2796.

(7) Zhu, Y.; Sheng, R.; Luo, T.; Li, H.; Sun, J.; Chen, S.; Sun, W.; Cao, A. Honeycomb-Structured Films by Multifunctional Amphiphilic Biodegradable Copolymers: Surface Morphology Control and Biomedical Application as Scaffolds for Cell Growth. *ACS Appl. Mater. Interfaces* **2011**, *3*, 2487−2495.

(8) Bunz, U. H. F. Breath Figures as a Dynamic Templating Method for Polymers and Nanomaterials. *Adv. Mater.* **2006**, *18*, 973−989.

(9) Hernández-Guerrero, M.; Stenzel, M. H. Honeycomb Structured Polymer Films via Breath Figures. *Polym. Chem.* **2012**, *3*, 563−577.

(10) Bai, H.; Du, C.; Zhang, A.; Li, L. Breath Figure Arrays: Unconventional Fabrications, Functionalizations, and Applications. *Angew. Chem., Int. Ed.* **2013**, *52*, 12240−12255.

(11) Lee, S. H.; Lee, D. H.; Lee, W. J.; Kim, S. O. Tailored Assembly of Carbon Nanotubes and Graphene. *Adv. Funct. Mater.* **2011**, *21*, 1338−1354.

(12) Lee, S. H.; Park, J. S.; Lim, B. K.; Mo, C. B.; Lee, W. J.; Lee, J. M.; Hong, S. H.; Kim, S. O. Highly Entangled Carbon Nanotube Scaffolds by Self-Organized Aqueous Droplets. *Soft Matter* **2009**, *5*, 2343−2346.

(13) Han, Y.; Zhang, Q.; Han, F.; Li, C.; Sun, J.; Lu, Y. Fabrication of Conducting Polypyrrole Film with Microlens Arrays by Combination of Breath Figures and Replica Molding Methods. *Polymer* **2012**, *53*, 2599−2603.

(14) Farbod, F.; Pourabbas, B.; Sharif, M. Direct Breath Figure Formation on PMMA and Superhydrophobic Surface Using In Situ Perfluoro-Modified Silica Nanoparticles. *J. Polym. Sci., Part B: Polym. Phys.* **2013**, *51*, 441−451.

(15) Huang, C.; Kamra, T.; Chaudhary, S.; Shen, X. Breath Figure Patterns Made Easy. *ACS Appl. Mater. Interfaces* **2014**, *6*, 5971−5976.

(16) Yabu, H.; Tanaka, M.; Ijiro, K.; Shimomura, M. Preparation of Honeycomb-Patterned Polyimide Films by Self-Organization. *Langmuir* **2003**, *19*, 6297−6300.

(17) Waters, C. M.; Bassler, B. L. Quorum Sensing: Cell-to-Cell Communication in Bacteria. *Annu. Rev. Cell Dev. Biol.* **2005**, *21*, 319−346.

(18) Okwumabua, O.; Shull, E.; O'Connor, M.; Moua, T. V.; Danz, T.; Strelow, K. Comparison of Three Methods for Extraction of Mycobacterium Avium Subspecies Paratuberculosis DNA for Polymerase Chain Reaction from Broth-Based Culture Systems. *J. Vet. Diagn. Invest.* **2010**, *22*, 67−69.

(19) Muñoz-Bonilla, A.; Ibarboure, E.; Bordegé, V.; Fernández-García, M.; Rodríguez-Hernández, J. Fabrication of Honeycomb-Structured Porous Surfaces Decorated with Glycopolymers. *Langmuir* **2010**, *26*, 8552−8558.

(20) Lu, Y.; Zhao, B.; Ren, Y.; Xiao, G.; Wang, X.; Li, C. Water-Assisted Formation of Novel Molecularly Imprinted Polymer Membranes with Ordered Porous Structure. *Polymer* **2007**, *48*, 6205−6209.

(21) Xu, S.; Lu, H.; Li, J.; Song, X.; Wang, A.; Chen, L.; Han, S. Dummy Molecularly Imprinted Polymers-Capped CdTe Quantum Dots for the Fluorescent Sensing of 2,4,6-Trinitrotoluene. *ACS Appl. Mater. Interfaces* **2013**, *5*, 8146−8154.

(22) Lee, M.-H.; Thomas, J. L.; Chen, Y.-C.; Wang, H.-Y.; Lin, H.-Y. Hydrolysis of Magnetic Amylase-Imprinted Poly(ethylene-*co*-vinyl alcohol) Composite Nanoparticles. *ACS Appl. Mater. Interfaces* **2012**, *4*, 916−921.

(23) Ma, Y.; Pan, G.; Zhang, Y.; Guo, X.; Zhang, H. Narrowly Dispersed Hydrophilic Molecularly Imprinted Polymer Nanoparticles for Efficient Molecular Recognition in Real Aqueous Samples Including River Water, Milk, and Bovine Serum. *Angew. Chem., Int. Ed.* **2013**, *52*, 1511−1514.

(24) Tokonami, S.; Shiigi, H.; Nagaoka, T. Review: Micro- and Nanosized Molecularly Imprinted Polymers for High-Throughput Analytical Applications. *Anal. Chim. Acta* **2009**, *641*, 7−13.

(25) Shen, X.; Xu, C.; Uddin, K. M. A.; Larsson, P.-O.; Ye, L. Molecular Recognition with Colloidosomes Enabled by Imprinted Polymer Nanoparticles and Fluorogenic Boronic acid. *J. Mater. Chem. B* **2013**, *1*, 4612−4618.

(26) Xu, C.; Uddin, K. M. A.; Shen, X.; Surangi, H.; Jayawardena, N.; Yan, M.; Ye, L. Photoconjugation of Molecularly Imprinted Polymer with Magnetic Nanoparticles. *ACS Appl. Mater. Interfaces* **2013**, *5*, 5208−5213.

(27) Shen, X.; Ye, L. Interfacial Molecular Imprinting in Nanoparticle-Stabilized Emulsions. *Macromolecules* **2011**, *44*, 5631−5637.

(28) Shen, X.; Zhou, T.; Ye, L. Molecular Imprinting of Protein in Pickering Emulsion. *Chem. Commun.* **2012**, *48*, 8198−8200.

(29) Hajizadeh, S.; Xu, C.; Kirsebom, H.; Ye, L.; Mattiasson, B. Cryogelation of Molecularly Imprinted Nanoparticles: A Macroporous Structure as Affinity Chromatography Column for Removal of β-Blockers from Complex Samples. *J. Chromatogr., A* **2013**, *1274*, 6−12.

(30) Wan, L.; Ke, B.; Li, X.; Meng, X.; Zhang, L.; Xu, Z. Honeycomb-Patterned Films of Polystyrene/Poly(ethylene glycol): Preparation, Surface Aggregation and Protein Adsorption. *Sci. China, Ser. B: Chem.* **2009**, *52*, 969−974.

(31) Shen, X.; Ye, L. Molecular Imprinting in Pickering Emulsions: A New Insight into Molecular Recognition in Water. *Chem. Commun.* **2011**, *47*, 10359−10361.

(32) Zhou, T.; Shen, X.; Chaudhary, S.; Ye, L. Molecularly Imprinted Polymer Beads Prepared by Pickering Emulsion Polymerization for Steroid Recognition. *J. Appl. Polym. Sci.* **2014**, *131*, 39606.

(33) Huang, C.; Shen, X. Janus Molecularly Imprinted Polymer Particles. *Chem. Commun.* **2014**, *50*, 2646−2649.

(34) Nagpal, M.; Singh, S. K.; Mishra, D. Superporous Hybrid Hydrogels Based on Polyacrylamide and Chitosan: Characterization and in vitro Drug Release. *Int. J. Pharm. Invest.* **2013**, *3*, 88−94.

(35) Huang, C.; Tu, Z.; Shen, X. Molecularly Imprinted Photocatalyst with a Structural Analogue of Template and Its Application. *J. Hazard. Mater.* **2013**, *248−249*, 379−386.

(36) Zhang, Y.; Guan, Y.; Zhou, S. Synthesis and Volume Phase Transitions of Glucose-Sensitive Microgels. *Biomacromolecules* **2006**, *7*, 3196−3201.

(37) Sharma, V.; Song, L.; Jones, R. L.; Barrow, M. S.; Williams, P. R. Srinivasarao, Effect of Solvent Choice on Breath-Figure-Templated Assembly of "Holey" Polymer Films. *Europhys. Lett.* **2010**, *91*, 38001.

(38) Park, M. S.; Kim, J. K. Breath Figure Patterns Prepared by Spin Coating in a Dry Environment. *Langmuir* **2004**, *20*, 5347−5352.

(39) Park, M. S.; Joo, W.; Kim, J. K. Porous Structures of Polymer Films Prepared by Spin Coating with Mixed Solvents under Humid Condition. *Langmuir* **2006**, *22*, 4594−4598.

(40) Wu, C. Y.; Chiang, T. H.; Hsu, C.-C. Fabrication of Microlens Array Diffuser Films with Controllable Haze Distribution by Combination of Breath Figures and Replica Molding Methods. *Opt. Express* **2008**, *16*, 19978−19986.

(41) Sun, W.; Ji, J.; Shen, J. Rings of Nanoparticle-Decorated Honeycomb-Structured Polymeric Film: The Combination of Pickering Emulsions and Capillary Flow in the Breath Figures Method. *Langmuir* **2008**, *24*, 11338−11341.
(42) Binks, B. P. Particles as Surfactants-Similarities and Differences. *Curr. Opin. Colloid Interface Sci.* **2002**, *7*, 21−41.
(43) Sun, W.; Shao, Z.; Ji, J. Particle-Assisted Fabrication of Honeycomb-Structured Hybrid Films via Breath Figures Method. *Polymer* **2010**, *51*, 4169−4175.
(44) Connal, L. A.; Vestberg, R.; Hawker, C. J.; Qiao, G. G. Dramatic Morphology Control in the Fabrication of Porous Polymer Films. *Adv. Funct. Mater.* **2008**, *18*, 3706−3714.
(45) Wang, H. Y.; Kobayashi, T.; Fujii, N. Preparation of Molecular Imprint Membranes by the Phase Inversion Precipitation Technique. *Langmuir* **1996**, *12*, 4850−4856.
(46) Kobayashi, T.; Fukaya, T.; Abe, M.; Fujii, N. Phase Inversion Molecular Imprinting by Using Template Copolymers for High Substrate Recognition. *Langmuir* **2002**, *18*, 2866−2872.